Phase Segregation on Different Length Scales in a Model Cell Membrane System

Jian Liu,[†] Shuyan Qi,[‡] Jay T. Groves,[†,§,||] and Arup K. Chakraborty*[,†,‡,§,||,⊥]

Department of Chemistry, Department of Chemical Engineering, and Biophysics Graduate Group, University of California, Berkeley, California 94720, and Physical Biosciences and Materials Sciences Division, Lawrence Berkeley National Laboratory, Berkeley, California 94720

Received: June 29, 2005

Lipid rafts are sphingolipid- and cholesterol-enriched domains on cell membranes that have been implicated in many biological functions, especially in T lymphocytes. We used a field theory to examine the forces underlying raft formation on resting living cell membranes. We find that it is difficult to reconcile the observed size of rafts on living cell membranes (∼100 nm) with a mechanism that involves coupling between spontaneous curvature differences and concentration fluctuations. Such a mechanism seems to predict raft domain sizes that are larger and commensurate with those observed on synthetic membranes. Therefore, using a Poisson−Boltzmann approach, we explore whether electrostatic forces originating from transmembrane proteins and net negative charges on cell membranes could play a role in determining the raft size in living cell membranes. We find that a balance among the intrinsic tendency of raft components to segregate, the line tension, and the effective dipolar interactions among membrane constituents leads to a stable phase with a characteristic length scale commensurate with the observed size of rafts on living cell membranes. We calculate the phase diagram of a system in which these three types of forces are important. In a certain region of the parameter space, an interesting phase with mosaic-like morphology consisting of an intertwined pattern of raft and nonraft domains is predicted. Experiments that could further assess the importance of dipolar interactions for lateral organization of the components on multiple length scales in membranes are suggested.

Introduction

Cell membranes are multicomponent mixtures of different types of lipids, cholesterol, and proteins.[1] The lateral organization of various components into domains is thought to be important for biological functions that include endocytosis, signaling, and protein transport.[2−5] Lipid rafts are typically defined as domains on cell membranes that are enriched in cholesterol, sphingolipids, and certain proteins.[2,5] Both the lipid raft domains and the matrix in which they are embedded are fluid under the usual physiological conditions.[3] It has been widely speculated that lipid rafts play a role in protein sorting and cell signaling.[2,5] For example, the role of lipid rafts in signaling in B cells and in T cells has been debated vigorously.[6,7] Although the role of lipid rafts in mediating cell signaling remains unresolved, recent experiments have characterized their morphology in resting cells as well as in cells stimulated by receptor cross-linking or antigen challenge.[8−11] At first, the size of lipid rafts in resting cell membranes was controversial.[12] On the basis of careful experiments, it is now widely accepted that these domains are approximately 100 nm or smaller in size.[13−16]

There is also evidence for a hierarchy of lipid raft organization over multiple length scales. In synthetic lipid bilayers, it has been demonstrated that there are two distinct correlation length scales (∼100 nm and ∼1 μm) corresponding to phase-separated structures involving lipid rafts.[17,18] Experiments with living cells[10,15,19] also indicate that lipid rafts can cluster to form micrometer-sized domains that are not homogeneous, but instead consist of intertwined patterns formed by raft and nonraft domains. The mechanism of lipid raft clustering is unknown.

In this paper, by investigating an ideal three-component membrane system, we examine the thermodynamic forces that may lead to the lateral segregation of lipid raft components, and estimate the natural length scales associated with so-formed patterns. Our field-theoretic treatment suggests that the size of lipid rafts in cell membranes may be determined by the interplay among long-range dipolar interactions between the constituents, line tension between the raft and nonraft components, and thermodynamic forces driving the segregation of proteins that constitute the raft components from other constituents of cell membranes. This finding highlights the importance of the distribution of charges and that of dipole moments in the transmembrane domains of proteins[20,21] in mediating the lateral organization of cell membrane domains. We compute the phase diagram of a two-dimensional system in which dipolar interactions between the constituents may be important. In a certain region of the parameter space, we also find a thermodynamic instability that results in a mosaic-like morphology with a much larger length scale. This resembles the clustering of lipid raft domains observed on cell surfaces upon stimulating or cross-linking receptors.[10] Although this thermodynamic instability may not be connected to lipid raft clustering in living cells, our finding suggests further experiments with synthetic lipid bilayers.

Theoretical Model

For simplicity, we model a resting cell membrane as a two-dimensional, three-component system. Certain proteins, such as Lck, GPI-anchored proteins, etc., have been shown to have

* Corresponding author: arup@uclink.berkeley.edu.
[†] Department of Chemistry, University of California.
[‡] Department of Chemical Engineering, University of California.
[§] Biophysics Graduate Group, University of California.
[||] Physical Biosciences, Lawrence Berkeley National Laboratory.
[⊥] Materials Sciences Division, Lawrence Berkeley National Laboratory.

10.1021/jp053562j CCC: $30.25
Published on Web 10/04/2005

a high affinity for raft domains.[10,11] Thus, in our coarse-grained field theory, we consider these "constitutive" raft proteins, sphingolipids, and cholesterols to be the raft component, A. Outside of lipid rafts, cell membranes are still heterogeneous.[22] Some proteins, e.g., CD45 and CD71 in T cells,[10,11] are known to always be excluded from lipid raft domains. Therefore, we denote these nonraft proteins and associated lipids to be the nonraft component, B, as distinct from the background component, C.

We assume that the raft and nonraft components have an intrinsic tendency to phase-separate from each other. The driving forces for phase separation could originate from many possible physical effects. For example, lipid raft components could be stiffer than the surrounding lipids.[3,23] Hence, a fluctuation-induced interaction[24] could exist between the lipid raft components. Alternatively, they could prefer different orientations, or there could be hydrophobic mismatches.[25] We model this intrinsic tendency to phase-separate using a Flory−Huggins approximation.

Another physical effect that may lead to phase segregation of certain proteins in cell membranes is the differential spontaneous curvature preferences of different components. As has been demonstrated before,[36] this introduces a coupling between concentration fluctuations and membrane-shape fluctuations.

As we show in the next section, inclusion of just these interactions does not seem to be consistent with the measured size of rafts. Our quest for understanding the forces that drive raft formation has led us to consider electrostatic interactions between components. Because cell membranes are embedded in ionic solutions, electrostatic interactions in solutions are usually effective only within the screening length (which is about 1−10 nm under physiological conditions). However, long-range dipolar interactions between membrane components may still be relevant for the following reasons. First of all, many transmembrane proteins exhibit α-helical motifs within the transmembrane domain.[1] The dipole moment of a helix is on the order of tens of debyes (estimated from Ben-Tal and Honig[26] and van Holde et al.[27]). As shown in Appendix 1, although the screening effect in the adjacent solution renormalizes the dipolar interactions between these helices, it cannot completely screen out these long-range dipolar interactions. This is because the α-helical dipoles are immersed in the finite-sized nonionic low-dielectric medium within the membrane. Therefore, although weaker due to the screening outside the membrane, the dipolar interactions between helices remain effective. Upon stimulation, membrane proteins can undergo conformational changes,[28] and may have vertical piston-like movements.[29] These modifications may initiate and/or vary the long-range dipolar interactions. Another possible source of effective dipolar interactions needs to be considered as well. In Appendix 2, we show that the long wavelength fluctuations (longer than the screening length) of the net surface charges on cell membranes yield an effective long-range dipolar-like interaction in a salty solution. Our results can be reduced to those obtained by Andelman et al.[30] in the limit of a large membrane width. The net surface charge on cell membranes (0.3−0.8 e/nm^2) may come from the negatively charged phosphatidylserine and membrane proteins.[31−35]

Thus, we have three types of interactions that may influence the formation and size of lipid raft domains on cell membranes: intrinsic tendency for certain proteins to aggregate, long-range repulsive dipolar interactions, and spontaneous curvature differences coupled to concentration fluctuations. The interplay between these effects and the line tension between phases enriched in particular components will set the length scales characterizing lipid raft domains. Therefore, to investigate the phase diagram and the length scales characterizing microdomain formation on cell membranes, we consider the following free energy

$$F = \int d\vec{x}_1 \int d\vec{x}_2 \sum_{i,j} \frac{d_i d_j \rho_i(\vec{x}_1)\rho_j(\vec{x}_2)}{4\pi\epsilon_{\text{membrane}}\epsilon_0(\vec{x}_1 - \vec{x}_2)^3} + \frac{1}{2}\int d\vec{x}\{\sigma(\nabla h(\vec{x}))^2 + \kappa(\nabla^2 h(\vec{x}))^2 + \sum_i H_i\kappa\rho_i(\vec{x})\nabla^2 h(\vec{x})\} + \frac{1}{2}\int d\vec{x}\sum_i \gamma_i(\nabla\rho_i(\vec{x}))^2 + \int d\vec{x}\{\sum_i \rho_i(\vec{x}) \ln \rho_i(\vec{x}) + \sum_{i,j}\chi_{ij}\rho_i(\vec{x})\rho_j(\vec{x})\} \quad (1)$$

where the free energy is scaled by k_BT, the lengths are scaled by the square root of the elementary area of a single component, $\rho_i(\vec{x})$ is the local concentration for species i, ϵ_0 is the electric permittivity in a vacuum, the effective dielectric constant of the membrane is $\epsilon_{\text{membrane}} = 3$, d_i is the normal component of the effective dipole moment carried by species i, γ_i is the interfacial line tension parameter, $\chi_{ij}(T)$ is the Flory−Huggins interaction parameter between species i and j and is a function of temperature, $h(\vec{x})$ is the membrane height fluctuation in the Monge gauge,[37] σ is the surface tension of the cell membrane ($\sigma = 3.1 \times 10^{-6}$ N/m[38,39]), κ is the bending rigidity of the cell membranes (κ = 100's k_BT[38,39]), and H_i is the spontaneous curvature for pure species i. Korlach et al.[40] have shown that the opposing leaflets of lipid bilayers are strongly coupled during phase separation. Hence, qualitatively, the lipid bilayer behaves like a monolayer, and so we do not treat the bilayer feature of the membranes.

Close to the critical point, by expanding the concentration fields around their mean values, we obtain the following Landau free energy functional up to the quartic order (ignoring the constant term)

$$F = \int d\vec{x}_1 \int d\vec{x}_2 \sum_{i,j}^{A,B} \frac{D_i D_j \psi_i(\vec{x}_1)\psi_j(\vec{x}_2)}{(\vec{x}_1 - \vec{x}_2)^3} + \frac{1}{2}\int d\vec{x}\{(\gamma_A + \gamma_C)(\nabla\psi_A(\vec{x}))^2 + (\chi_A + \chi_C)\psi_A(\vec{x})^2 + (\gamma_B + \gamma_C)(\nabla\psi_B(\vec{x}))^2 + (\chi_B + \chi_C)\psi_B(\vec{x})^2 + (2\gamma_C)(\nabla\psi_A(\vec{x}))(\nabla\psi_B(\vec{x})) + 2\chi_C\psi_A(\vec{x})\psi_B(\vec{x})\} + \frac{1}{2}\int d\vec{x}\{\sigma(\nabla h(\vec{x}))^2 + \kappa(\nabla^2 h(\vec{x}))^2 + (S_A\psi_A(\vec{x}) + S_B\psi_B(\vec{x}))(\nabla^2 h(\vec{x}))\} + \int d\vec{x}\{A_3\psi_A(\vec{x})^3 + B_3\psi_B(\vec{x})^3 - C_3(\psi_A(\vec{x}) + \psi_B(\vec{x}))^3 + A_4\psi_A(\vec{x})^4 + B_4\psi_B(\vec{x})^4 + C_4(\psi_A(\vec{x}) + \psi_B(\vec{x}))^4\} \quad (2)$$

where $\psi_i(\vec{x}) = (\rho_i(\vec{x}) - \bar{\rho}_i)/\rho_{\text{total}}$, $\rho_{\text{total}} = \sum_i \rho_i(\vec{x}) = 1$, $\bar{\rho}_i$ is the average concentration for species i. We consider the incompressibility condition $\psi_A(\vec{x}) + \psi_B(\vec{x}) + \psi_C(\vec{x}) = 0$. $\chi_A = \chi_{AA} + \chi_{CC} - 2\chi_{AC} + 1/2\bar{\rho}_A + 1/2\bar{\rho}_C$, $\chi_B = \chi_{BB} + \chi_{CC} - 2\chi_{BC} + 1/2\bar{\rho}_B + 1/2\bar{\rho}_C$, and $\chi_C = \chi_{AB} + \chi_{CC} - \chi_{BC} - \chi_{AC} + 1/2\bar{\rho}_C$. Also, $A_3 = (-1/6)(1/\bar{\rho}_A{}^2)$, $B_3 = (-1/6)(1/\bar{\rho}_B{}^2)$, $C_3 = (-1/6)(1/\bar{\rho}_C{}^2)$, $A_4 = (1/12)(1/\bar{\rho}_A{}^3)$, $B_4 = (1/12)(1/\bar{\rho}_B{}^3)$, $C_4 = (1/12)(1/\bar{\rho}_C{}^3)$. $D_A = (d_A - d_C)/\sqrt{4\pi\epsilon_0\epsilon_{\text{membrane}}}$, $D_B = (d_B - d_C)/\sqrt{4\pi\epsilon_0\epsilon_{\text{membrane}}}$, S_A

$= (H_A - H_C)\kappa$, $S_B = (H_B - H_C)\kappa$. This free energy functional is the basis for all our results.

Results

Coupling of Spontaneous Curvature and Concentration Fluctuations May Not Be Important for Lipid Raft Formation in Cell Membranes. Let us first examine whether the coupling between concentration fluctuations and membrane shape, resulting from differences in spontaneous curvature between the raft components and others, can lead to domain sizes that are commensurate with the observed size of the rafts. For theoretical simplicity, we consider this question for a two-component system (raft components (A) and background lipids (C)). Our numerical calculations for a three-component system led us to qualitatively the same conclusion as that obtained for a two-component system.

For a two-component system without dipolar interactions, eq 2 can be simplified to obtain

$$F = \int d\vec{x} \frac{1}{2}\{\gamma(\nabla\psi_A(\vec{x}))^2 + \tau\,\psi_A(\vec{x})^2\} + \frac{1}{2}\{\sigma(\nabla h(\vec{x}))^2 + \kappa(\nabla^2 h(\vec{x}))^2\} + S_A\,\psi_A(\vec{x})\nabla^2 h(\vec{x}) + F_{\text{higher-order}} \quad (3)$$

We can average over the membrane shape fluctuations exactly to obtain the following effective free energy

$$F = \frac{1}{2}\int d\vec{q}\left\{\gamma q^2 - \frac{S_A{}^2 q^2}{\sigma + \kappa q^2} + \tau\right\}\psi_A(\vec{q})\,\psi_A(-\vec{q}) + F_{\text{higher-order}} \quad (4)$$

When $S_A{}^2 < \sigma\kappa$, there are no concentration fluctuations over a finite length scale. For $S_A{}^2 > \sigma\kappa$, there is a free energy minimum corresponding to the optimal wavelength $\sim 2\pi/q^*$, which characterizes the linear size of the so-formed phase

$$q^* = \sqrt{\frac{S_A\sqrt{\frac{\sigma}{\gamma}} - \sigma}{\kappa}} \quad (5)$$

By choosing the optimal domain size to be the observed linear size of lipid rafts ($\sim$100 nm), and taking the typical values $\gamma = 5k_BT$,[43,44] $\kappa = 400k_BT$,[38,39] and $\sigma = 3.1 \times 10^{-6}$ N/m[38,39] (all the parameters are for cell membranes), we found the required spontaneous curvature difference to be on the order of 330 μm^{-1}.

In experiments wherein synthetic lipid membranes undergo a budding transition, mother vesicles enriched in background phospholipids and daughter vesicles enriched in the lipid raft component are both on the order of micrometers in size.[23,41] The sizes of these vesicles should be approximately equal to the inverse of the spontaneous curvature for the corresponding membrane domains. This implies that the spontaneous curvature for cholesterol-enriched raft domains (A) and that of the background phospholipid domains (C) must be on the order of or less than 1 μm^{-1}. (The detailed calculations are given in Appendix 3.) Therefore, the spontaneous curvature difference between lipid raft components (A) and the background phospholipids (C), $H_A - H_C$, is about 1 μm^{-1}. This estimate is also in agreement with experimental studies of the spontaneous curvature ($\sim$1.6 μm^{-1}) of synthetic vesicles induced by ganglioside GM-1, the glycolipid constituent of lipid rafts.[42] In this experiment, the concentration of GM-1 is roughly the same as physiological levels.[1] Therefore, the required spontaneous curvature difference (330 μm^{-1}) for 100 nm rafts is 2 orders of magnitude larger than the typical experimental measures of spontaneous curvature (1 μm^{-1}) because of the coupling between spontaneous curvature differences and concentration fluctuations.

These results lead us to suggest that the coupling between spontaneous curvature differences and concentration fluctuations may not be important in determining the formation of lipid raft domains ($\sim$100 nm) on living cell membranes. It is, however, likely to be the dominant physical effect controlling raft formation on synthetic lipid membranes[23] (see Appendix 3 for details).

Long-Range Dipolar Interactions Could Result in a Disorder−Order Phase Transition with a Characteristic Length Scale Commensurate with the Size of Rafts on Living Cell Membranes. Given the results above, we now consider eq 2 without the spontaneous curvature terms. After Fourier transformation, we obtain

$$F = \frac{1}{2}\int d\vec{q}\{A_2(q)\,\psi_A(\vec{q})\,\psi_A(-\vec{q}) + B_2(q)\,\psi_B(\vec{q})\,\psi_B(-\vec{q}) + C_2(q)\,\psi_A(\vec{q})\,\psi_B(-\vec{q})\} + F_{\text{higher-order}} \quad (6)$$

where

$$A_2(\vec{q}) = (\gamma_A + \gamma_C)q^2 - D_A{}^2 q + \tau_A + \tau_C$$

$$B_2(\vec{q}) = (\gamma_B + \gamma_C)q^2 - D_B{}^2 q + \tau_B + \tau_C$$

$$C_2(\vec{q}) = 2\gamma_C q^2 - 2D_A D_B q + 2\tau_C$$

The modified Flory−Huggins parameter τ_i consists of the original Flory−Huggins interaction χ_i and the average dipole−dipole repulsion, and it is proportional to inverse temperature. We estimate the parameters according to the values found in the literature that are relevant to physiological conditions. We choose $\gamma_A = \gamma_B = \gamma_C = 10^{-11}$ N,[43,44] and take $|\tau_A| = |\tau_B| = |\tau_C| = 0.1$ (close to instability). By varying the parameters γ_A, γ_B, and γ_C independently within the same order of magnitude, we find qualitatively similar results. To simplify the analysis, we choose $\gamma_A = \gamma_B = \gamma_C = \gamma$. Similarly, we also choose $\tau_A = \tau_B = \tau_C = \tau$ for most cases. Since most transmembrane proteins are either in the raft domains (A) or in the nonraft domain (B), we expect domains A and B to have a larger effective dipole moment than the background domain C that is composed of phospholipids. Thus we choose D_A, D_B = 10's of debyes.[26,27]

We first discuss the nature of the instability arising from the disordered phase. Diagonalizing the quadratic term of the free energy functional in eq 6, we obtain

$$F_2 = (\Phi_1(\vec{q})\ \Phi_2(\vec{q}))\begin{pmatrix}\lambda_1(\vec{q}) & 0\\ 0 & \lambda_2(\vec{q})\end{pmatrix}\begin{pmatrix}\Phi_1(-\vec{q})\\ \Phi_2(-\vec{q})\end{pmatrix} \quad (7)$$

$$\Phi_1 = e_1\psi_A + \psi_B$$

$$e_1 = \frac{1}{2C_2(q)}[A_2(q) - B_2(q) - \sqrt{(A_2(q) - B_2(q))^2 + 4C_2(q)^2}]$$

$$\lambda_1(q) = \frac{1}{2}[A_2(q) + B_2(q) - \sqrt{(A_2(q) - B_2(q))^2 + 4C_2(q)^2}]$$

$$\Phi_2 = e_2\psi_A + \psi_B$$

$$e_2 = \frac{1}{2C_2(q)}[A_2(q) - B_2(q) + \sqrt{(A_2(q) - B_2(q))^2 + 4C_2(q)^2}]$$

$$\lambda_2(q) = \frac{1}{2}[A_2(q) + B_2(q) + \sqrt{(A_2(q) - B_2(q))^2 + 4C_2(q)^2}]$$

Minimizing the two eigenvalues $\lambda_1(q)$ and $\lambda_2(q)$, we obtain the wavevectors corresponding to the optimal sizes of concentration fluctuations, $2\pi/q^*$ and $2\pi/Q^*$. The corresponding eigenvectors ($\Phi_1(q^*)$, $\Phi_2(q^*)$) and ($\Phi_1(Q^*)$, $\Phi_2(Q^*)$) reflect the modes of segregation among the three components.

Figure 1 shows that, when the difference between the effective dipole moments of the components that constitute the lipid raft phase and the background lipids exceeds a threshold value, the homogeneous phase becomes unstable ($\lambda_1(q^*) < 0$). This will lead to a disorder−order phase transition, and the ordered phase reflects a separation between the raft component (A) and other components (B and C). As shown later, the length scale characterizing the instability is commensurate with the measured size of lipid rafts on cell membranes.

To establish these results more concretely, we also calculated the phase diagram and studied the ordered phases. Within a one wavenumber approximation, there are two basic phases for two-dimensional patterns: the stripe and the hexagonal. The order parameters characterizing the two phases can be written as follows

$$\psi_A(\vec{x}) = \sqrt{\frac{2}{n}}a\sum_{i=1}^{n}(e^{i(\vec{q}_i\vec{x}+\alpha_i)} + e^{-i(\vec{q}_i\vec{x}+\alpha_i)})$$

$$\psi_B(\vec{x}) = \sqrt{\frac{2}{m}}b\sum_{i=1}^{n}(e^{i(\vec{q}_i\vec{x}+\beta_i)} + e^{-i(\vec{q}_i\vec{x}+\beta_i)})$$

where $n = 1$ ($m = 1$) represents the stripe phase, and $n = 3$ ($m = 3$) represents the hexagonal phase for component A (B) with $\sum_{i=1}^{3}\vec{q}_i = 0$. For simplicity, we set $\alpha_i = 0$ and $\beta_i = 0$. A and B may assume different symmetries ($n \neq m$). Substituting the order parameters into eq 7, we have

$$F_{SS} = 2(A_2(\vec{q})a^2 + B_2(\vec{q})b^2 + C_2(\vec{q})ab) + 24(A_4a^4 + B_4b^4 + C_4(a+b)^4)$$

$$F_{HS} = 2(A_2(\vec{q})a^2 + B_2(\vec{q})b^2) + \frac{2}{\sqrt{3}}C_2(\vec{q})ab + \frac{8}{3}\sqrt{6}A_3a^3 + 8\sqrt{2}a^2b + 40A_4a^4 + 24B_4b^4 + \frac{160}{\sqrt{3}}C_4a^3b + 64C_4a^2b^2 + \frac{96}{\sqrt{3}}C_4ab^3$$

$$F_{SH} = 2(A_2(\vec{q})a^2 + B_2(\vec{q})b^2) + \frac{2}{\sqrt{3}}C_2(\vec{q})ab + \frac{8}{3}\sqrt{6}B_3b^3 + 8\sqrt{2}ab^2 + 40B_4b^4 + 24A_4a^4 + \frac{160}{\sqrt{3}}C_4b^3a + 64C_4a^2b^2 + \frac{96}{\sqrt{3}}C_4ba^3$$

$$F_{HH} = 2(A_2(\vec{q})a^2 + B_2(\vec{q})b^2 + C_2(\vec{q})ab) + \frac{8}{3}\sqrt{6}(A_3a^3 + B_3b^3 - C_3(a+b)^3) + 40(A_4a^4 + B_4b^4 + C_4(a+b)^4)$$

where, for example, F_{SH} is the free energy function for a stripe (A) and hexagonal (B) phase. For the rest of the paper, we choose a system with $\bar{\rho}_A:\bar{\rho}_B:\bar{\rho}_C = 1:2:6$. (Different compositions yield similar results.)

By comparing F_{SS}, F_{SH}, F_{HS}, F_{HH}, and the free energy of the disordered state (which is taken to be zero), we obtain the equilibrium phase for a given set of conditions. The optimized amplitudes a and b and optimized wavevector q^* are obtained by minimizing the free energy. This leads us to obtain the phase diagram (D_A vs τ_i) shown in Figure 2.

Figure 3 shows that the optimal size of the lipid raft domains is relatively insensitive to the value of the parameter τ. If $\tau = 0.01$, and the effective dipole D_A is taken to be 15, 20, and 25 D, we find that the size of the raft domains ($\sim 2\pi/q^*$) is roughly 150, 90 and 50 nm, respectively. This is on the same order of magnitude as the measured elementary lipid raft size on living cell membranes.[14,17] These results lead us to suggest that dipolar interactions may be important in the formation of lipid raft domains on cell membranes.

The origin of the optimal size of lipid raft domains can be understood as follows. As τ decreases, one approaches the disorder−order phase transition. The line tension arising from the interfacial tension tends to minimize the phase boundary so as to avoid the energetically unfavorable contact between the two phases. Therefore, line tension prefers macroscopic domains. On the other hand, the long-range dipolar interaction is repulsive, and it prefers no domains at all. The balance of the two competing forces results in a domain size that is much smaller than that obtained from a mechanism in which the concentration fluctuations are coupled to the spontaneous curvature differences.

A Second Instability in the Hexagonal−Hexagonal Phase. The inset in Figure 1 shows another interesting prediction of the theory. As D_A increases beyond the onset of the thermodynamic instability we have discussed, a second instability with a much larger length scale appears (~ 1 μm, data not shown). To explore the possibility that a second instability occurs on the basis of the first ordered phase, without losing generality, we carried out a linear stability analysis on the hexagonal−hexagonal phase. First, we set

$$\psi_A(\vec{x}) = \sqrt{\frac{2}{n}}(a+\delta a_1)\sum_{i=1}^{n}(e^{i\vec{q}_i^*\vec{x}} + e^{-i\vec{q}_i^*\vec{x}}) + \sqrt{\frac{2}{n}}\delta a_2\sum_{i=1}^{n}(e^{i\vec{Q}_i\vec{x}} + e^{-i\vec{Q}_i\vec{x}})$$

$$\psi_B(\vec{x}) = \sqrt{\frac{2}{n}}(b+\delta b_1)\sum_{i=1}^{n}(e^{i\vec{q}_i^*\vec{x}} + e^{-i\vec{q}_i^*\vec{x}}) + \sqrt{\frac{2}{n}}\delta b_2\sum_{i=1}^{n}(e^{i\vec{Q}_i\vec{x}} + e^{-i\vec{Q}_i\vec{x}})$$

where $\{\vec{q}_i^*\} \cap \{\vec{Q}_i\} = \Phi$, $n = 3$, $\sum_{i=1}^{3}\vec{q}_i^* = 0$, and $\sum_{i=1}^{3}\vec{Q}_i = 0$.

The perturbations include fluctuations over the linear length scale of the initial ordered phase ($2\pi/q^*$) and those associated with a different length scale ($2\pi/Q$). For the hexagonal−hexagonal phase, the free energy change up to second order in fluctuations is

$$\delta F_{HH} = 2(A_2(q^*)(\delta a_1)^2 + B_2(q^*)(\delta b_1)^2 + C_2(q^*)(\delta a_1\delta b_1)) + \frac{8}{3}\sqrt{6}(3A_3a(\delta a_1)^2 + 3B_3b(\delta b_1)^2 - 3C_3(a+b)(\delta a_1+\delta b_1)^2) + 40(6A_4a^2(\delta a_1)^2 + 6B_4b^2(\delta b_1)^2 + 6C_4(a+b)^2(\delta a_1+\delta b_1)^2) + 2(A_2(Q)(\delta a_2)^2 + B_2(Q)(\delta b_2)^2 + C_2(Q)(\delta a_2\delta b_2)) + 96(A_4a^2(\delta a_2)^2 + B_4b^2(\delta b_2)^2 + C_4(a+b)^2(\delta a_2+\delta b_2)^2) \quad (8)$$

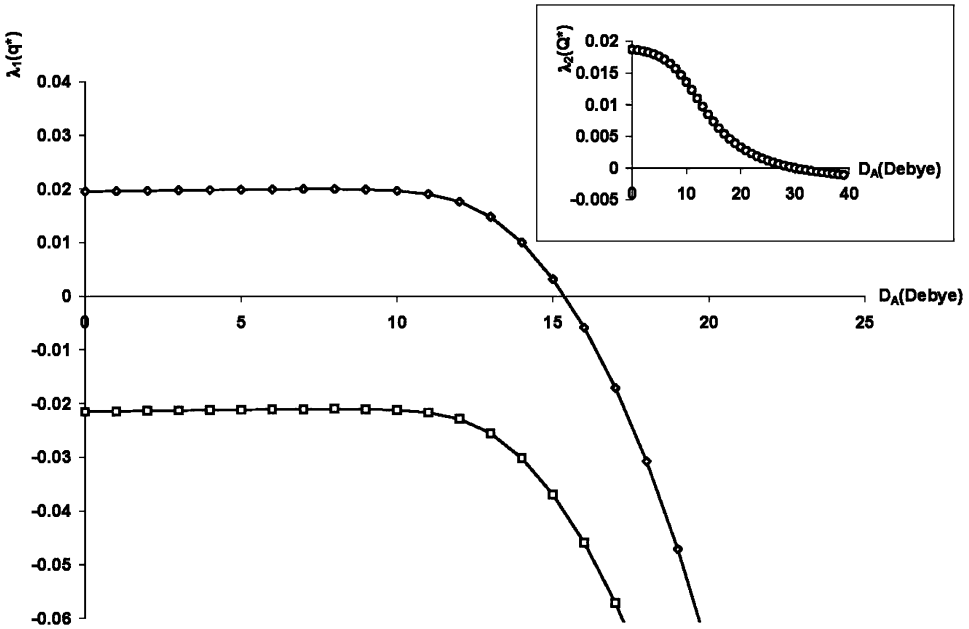

Figure 1. Dependence of the eigenvalues of eq 7 on the relative dipole moment D_A at the optimal wavevectors. λ_1 is the smallest eigenvalue, and belongs to the eigenvector corresponding to incipient raft formation. The inset shows how the second eigenvalue depends on D_A. ◇: $\tau_A = \tau_B = \tau_C = 0.01$. □ and the inset: $\tau_A = -0.01$, $\tau_B = -0.012$, $\tau_C = 0.01$. Other parameters are $D_B = 5$ D, $\sigma = 3.1$ μN/m, $\gamma = 5k_BT$.

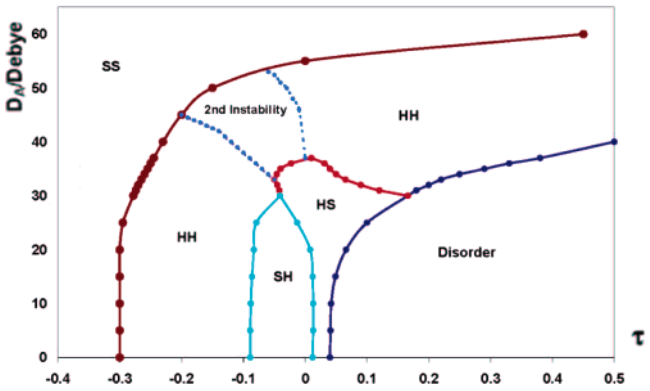

Figure 2. Phase diagrams (D_A vs τ_i) $\gamma = 5k_BT$, $D_B = 5$ D, $\bar{\rho}_A:\bar{\rho}_B:\bar{\rho}_C = 1:2:6$.

Notice that, up to second order in fluctuations, fluctuations over different length scales are totally decoupled (e.g., no $\delta a_1 \delta b_2$ or $\delta a_1 \delta a_2$ terms). It can also be shown that stripe-like perturbations ($n = 1$) result in exactly the same free energy change up to second order. So, from the standpoint of linear stability, the behavior is independent of the choice of specific symmetries of the phase-segregated patterns.

We can write eq 8 in matrix form as

$$\delta F_{HH} = (\delta a_1 \;\; \delta b_1 \;\; \delta a_2 \;\; \delta b_2)\begin{pmatrix} M_1 & 0 \\ 0 & M_2 \end{pmatrix}\begin{pmatrix} \delta a_1 \\ \delta b_1 \\ \delta a_2 \\ \delta b_2 \end{pmatrix}$$

where M_1 and M_2 are 2×2 matrixes as

Diagonalizing these matrixes, we get four eigenvalues: $\lambda_{11}(q^*)$ and $\lambda_{12}(q^*)$ for M_1, corresponding to the stability of the initial phases; $\lambda_{21}(Q)$ and $\lambda_{22}(Q)$ for M_2, which are signatures of the instability of perturbation modes with length scale equal to $2\pi/Q$. λ_{11} and λ_{12} are always positive. This means the initial hexagonal−hexagonal phases are always stable with respect to concentration fluctuations over the same length scale $\sim 2\pi/q^*$. We minimize λ_{21} and λ_{22} with respect to Q. In certain regions of the phase diagram (as shown in Figure 2), λ_{21} becomes negative, and fluctuations with a much larger optimal length scale $2\pi/Q^*$ ($Q^* \ll q^*$) become unstable. Therefore, while the initial hexagonal−hexagonal phase remains stable, the second instability emerges and leads to phase separation over a much larger length scale. On the basis of the analysis of the eigenvectors, the initial phase segregation caused by this second instability corresponds to the segregation of components A and B from the background component C. The separation modes could become more complicated when we vary the composition ratio of the system. Such a comprehensive study exploring various parameter ratios would be interesting to carry out in the future.

Next, we study the equilibrium phase in the region where large-scale patterns form, by allowing both δa_i and δb_i ($i = 1$ or 2) to evolve. We choose one point ($D_A = 40$ D, $\tau_i = -0.1$) in the phase diagram (see Figure 2), and obtain the equilibrium phase by minimizing the free energy. Because the system is now well into the ordered region, components A and B are strongly coupled, and one can show that the symmetry of phases rich in A and B are the same. Therefore, we ignore the cases in which the two components adopt different symmetries. We compare the free energy of hexagonal/hexagonal−hexagonal/

$$M_1 = \begin{pmatrix} 2A_2(q^*) + 8\sqrt{6}(A_3 a - C_3(a+b)) + 240(A_4 b^2 + C_4(a+b)^2) & C_2(q^*) - 8\sqrt{6}C_3(a+b) + 240C_4(a+b)^2 \\ C_2(q^*) - 8\sqrt{6}C_3(a+b) + 240C_4(a+b)^2 & 2B_2(q^*) + 8\sqrt{6}(B_3 b - C_3(a+b)) + 240(B_4 b^2 + C_4(a+b)^2) \end{pmatrix}$$

$$M_2 = \begin{pmatrix} 2A_2(Q) + 96(A_4 a^2 + C_4(a+b)^2) & C_2(Q) + 96C_4(a+b)^2 \\ C_2(Q) + 96C_4(a+b)^2 & 2B_2(Q) + 96(B_4 b^2 + C_4(a+b)^2) \end{pmatrix}$$

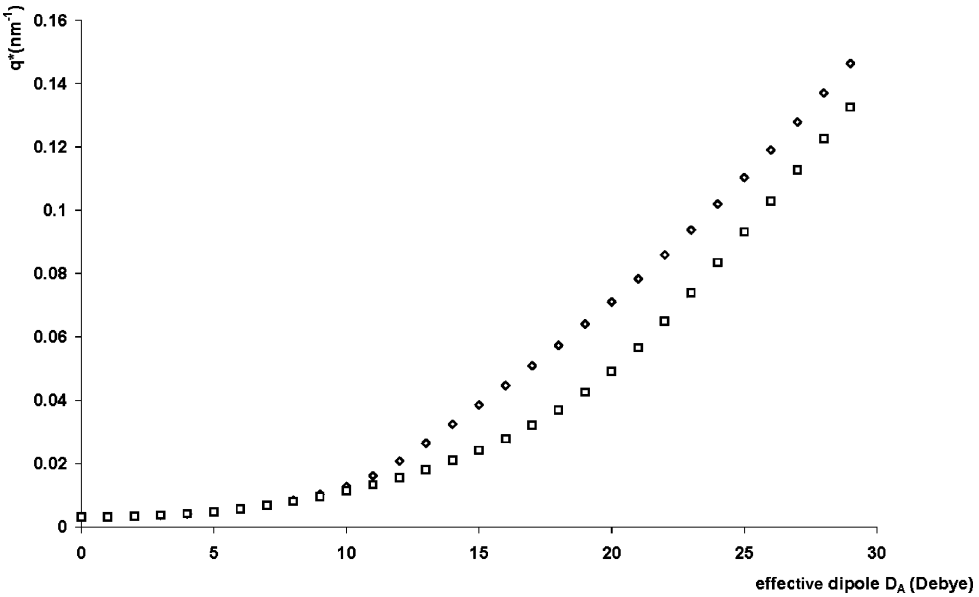

Figure 3. Dependence of the optimal wavenumber on the effective dipole strength D_A for different values of τ; a smaller value of τ implies a greater incompatibility. ◇: $\tau_A = \tau_B = \tau_C = 0.01$. □: $\tau_A = \tau_B = \tau_C = 0.1$.

hexagonal phases ($n = 3$, $m = 3$) and that of hexagonal/hexagonal−stripe/stripe phases ($n = 3$, $m = 1$).

$$\psi_A(\vec{x}) = \sqrt{\frac{2}{n}}a_1\sum_{i=1}^{n}(e^{i\vec{q}_i\vec{x}} + e^{-i\vec{q}_i\vec{x}}) + \sqrt{\frac{2}{m}}a_2\sum_{i=1}^{m}(e^{-i\vec{Q}_i\vec{x}} + e^{-i\vec{Q}_i\vec{x}})$$

$$\psi_B(\vec{x}) = \sqrt{\frac{2}{n}}b_1\sum_{i=1}^{n}(e^{i\vec{q}_i\vec{x}} + e^{-i\vec{q}_i\vec{x}}) + \sqrt{\frac{2}{m}}b_2\sum_{i=1}^{m}(e^{i\vec{Q}_i\vec{x}} + e^{-i\vec{Q}_i\vec{x}})$$

$$F_{HH-SS} = 2(A_2(q){a_1}^2 + B_2(q){b_1}^2 + C_2(q)a_1b_1 + A_2(Q){a_2}^2 + B_2(Q){b_2}^2 + C_2(Q)a_2b_2) + \frac{8}{3}\sqrt{6}(A_3{a_1}^3 + B_3{b_1}^3 - C_3(a_1 + b_1)^3) + 24(A_4{a_1}^4 + B_4{b_1}^4 + C_4(a_1 + b_1)^4) + 40(A_4{a_2}^4 + B_4{b_2}^4 + C_4(a_2 + b_2)^4) + 96(A_4{a_1}^2{a_2}^2 + B_4{b_1}^2{b_2}^2 + C_4(a_1 + b_1)^2(a_2 + b_2)^2)$$

$$F_{HH-HH} = 2(A_2(q){a_1}^2 + B_2(q){b_1}^2 + C_2(q)a_1b_1 + A_2(Q){a_2}^2 + B_2(Q){b_2}^2 + C_2(Q)a_2b_2) + \frac{8}{3}\sqrt{6}(A_3{a_1}^3 + B_3{b_1}^3 - C_3(a_1 + b_1)^3) + \frac{8}{3}\sqrt{6}(A_3{a_2}^3 + B_3{b_2}^3 - C_3(a_2 + b_2)^3) + 40(A_4{a_1}^4 + B_4{b_1}^4 + C_4(a_1 + b_1)^4) + 40(A_4{a_2}^4 + B_4{b_2}^4 + C_4(a_2 + b_2)^4) + 96(A_4{a_1}^2{a_2}^2 + B_4{b_1}^2{b_2}^2 + C_4(a_1 + b_1)^2(a_2 + b_2)^2)$$

For the chosen point, hexagonal/hexagonal−hexagonal/hexagonal phase is the most stable phase, and the corresponding equilibrium order parameters are

hexagonal phase 1: $q^* = 0.312\ \text{nm}^{-1}$, $a_1 = 0.0602$, $b_1 = -0.0106$

hexagonal phase 2: $Q^* = 0.007\ \text{nm}^{-1}$, $a_2 = 0.0023$, $b_2 = 0.0804$

Figure 4 shows the pattern of the total equilibrium concentration of components A and B. The raft (A) and nonraft (B) components are spatially segregated over the small length scale (∼20 nm), although they are both highly concentrated over the length scale of micrometers. So the mosaic-like pattern (∼0.9 μm) is enriched by lipid raft component A and nonraft components B, and depleted of background lipids C. This pattern resembles the observed lipid raft clustering.[10] However, the mechanisms that drive raft clustering in living cells are most likely quite different. Our results, however, do suggest interesting experiments with synthetic membrane systems.

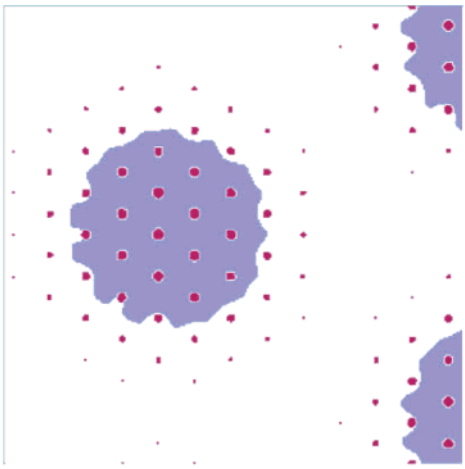

Figure 4. Mosaic-like pattern of raft clustering: Pink, raft domain; blue, nonraft domain; white, background in which both raft and nonraft components are depleted. (To have the best visualization effects, we artificially chose the concentration cutoff as follows: $\psi_A > 0.17$ as pink domains and $\psi_B > 0.08$ as blue domains.)

Summary

How spatial organization of cellular components influence cellular function is a subject of current attention.[45] Here, we used field-theoretic arguments to examine the influence of various forces in determining the ∼100 nm lipid raft domains formed on cell membranes. In particular, we studied a simple two-dimensional, three-component model system. Our results suggest that on resting cell membranes, the effective long-range dipolar interactions originating from the transmembrane regions of proteins and the net surface charges on cell membranes may

be important in determining the formation and size of lipid rafts. In contrast, microdomain formation on synthetic membrane systems that have been studied so far is more likely the result of coupling between concentration fluctuations and spontaneous curvature differences.

We have calculated the phase diagram of a three-component membrane system in which long-range dipolar interactions are important. According to the phase diagram, lipid rafts could emerge as a stable phase from the disordered state upon a temperature decrease and/or a relative effective dipole moment increase. Within the stable phase, lipid raft components segregate from the nonraft components and background lipids. The morphology of the stable phase can be either hexagonal droplet or stripe, depending on the extent of the phase segregation.

Our results also show that, under certain conditions, an intertwined mosaic-like phase that resembles raft clustering on cell membranes can form. This intertwined pattern has been observed in experiments on cell membranes upon cross-linking raft proteins or nonraft proteins,[10] and Dustin speculated that the immunological synapse may have such an intertwined mosaic-like morphology that it enables the dynamic contact of raft and nonraft proteins.[46] Although our mosaic-like phase may not be connected to such patterns formed on T cell membranes, could a synthetic membrane system be designed in which such a phase could result upon manipulating conditions such as temperature, ionic strength in the solution, or dipole moments? Could this then be a stimuli-responsive material?

Finally, some simplifications and assumptions adopted in our model are worth stating. First, there could be different types of lipid rafts in the same cell.[47,48] As a simple starting point, we do not discuss this complexity in our model. Second, we do not explicitly consider the internal texture of lipid rafts. The lipid raft domain is in the liquid ordered phase, and is closely packed. In addition, cholesterol is chiral.[3] Because we focus on the behavior of phase separation in cell membranes over relatively large length scales, we do not study this fine structure within lipid raft domains. Third, we did not consider chemical-reaction-induced differential partitioning of lipids between lipid raft and nonraft domains.[49] Also, we do not consider the case in which the nonraft proteins can enter lipid raft domains upon stimulation or chemical modification.[50,51]

Acknowledgment. This research is supported by the NSF through the Center for Polymer Interfaces and Macromolecular Assemblies and the QB3 Institute at University of California. Fruitful discussions with Prof. M. L. Dustin are gratefully acknowledged.

Appendix 1

Analysis of Dipoles Buried inside the Membrane. Consider electrostatic interactions between the dipole moments buried inside the membrane. The dipoles are effectively located on the same flat plane inside the membrane (as shown in Figure 5). They are preferentially oriented perpendicular to the midplane of the membrane when their average tangential components vanish. The two-dimensional polarization is given by $P = \mu\Phi$, where Φ is the in-plane monolayer concentration of the dipoles. The concentration, Φ, modulates a wave vector q: $\Phi(x) = \Phi_0 + \Phi_q e^{iqx}$. The ionic solution outside the membrane is characterized by the Debye−Hückel screening length κ^{-1} and the bulk

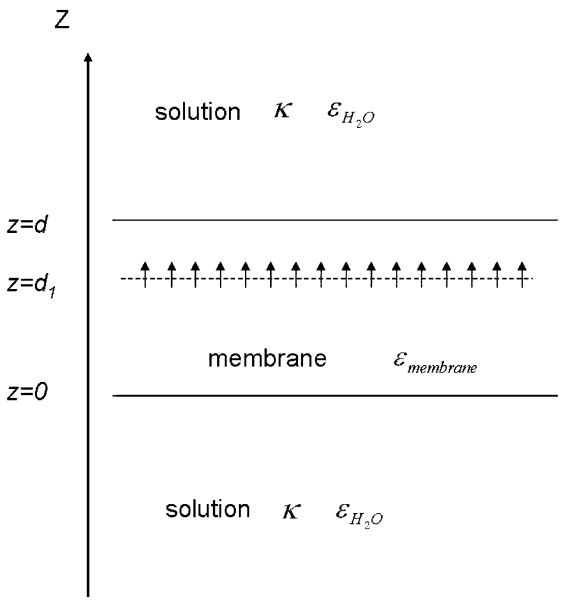

Figure 5. Schematic illustration of dipoles buried inside the membrane surrounded by the salty solution.

dielectric constant ϵ_{H_2O}. The discontinuity of the potential across the plane within the membrane where the dipoles reside is

$$\Delta V = \frac{P}{\epsilon_{\text{membrane}}} \tag{9}$$

The electrical potential V satisfies the linearized Poisson−Boltzmann equation

$$\nabla^2 V_1 - \kappa^2 V_1 = 0, z > d \tag{10}$$

$$\nabla^2 V_2 = 0, d_1 < z < d \tag{11}$$

$$\nabla^2 V_3 = 0, 0 < z < d_1 \tag{12}$$

$$\nabla^2 V_4 - \kappa^2 V_4 = 0, z < 0 \tag{13}$$

with the following boundary conditions:

$$\text{(i)} \lim_{z\to\infty} V_1 = \lim_{z\to-\infty} V_4 = 0$$

$$\text{(ii)} \epsilon_{H_2O}\frac{\partial V_1}{\partial z} = \epsilon_{\text{membrane}}\frac{\partial V_2}{\partial z}, z = d$$

$$\epsilon_{\text{membrane}}\frac{\partial V_2}{\partial z} = \epsilon_{\text{membrane}}\frac{\partial V_3}{\partial z}, z = d_1$$

$$\epsilon_{\text{membrane}}\frac{\partial V_3}{\partial z} = \epsilon_{H_2O}\frac{\partial V_4}{\partial z}, z = 0$$

$$\text{(iii)} V_1 = V_2, z = d$$

$$V_2 - V_3 = \Delta V, z = d_1$$

$$V_3 = V_4, z = 0$$

where d is the thickness of the membrane. We can calculate the potentials, and solve for the electrostatic free energy of the dipoles subject to these potentials to obtain

$$F_{\text{el}} = -\frac{1}{2}\int \vec{P}\vec{E}\, d\vec{r} = -\frac{1}{2}\int P\frac{\partial V_2}{\partial z}\, d\vec{r}, \text{ at } z = d_1 \tag{14}$$

In the limit of $q \ll \kappa$ (i.e., the concentration fluctuations oscillate over a much larger length scale than the screening length, or the high salt concentration limit), up to linear order in q, the free energy is

$$F_{\mathrm{el}}(q) = -\frac{1}{22\epsilon_{\mathrm{membrane}}}\frac{\mu^2\Phi_q{}^2}{}q\left(\frac{(1+e^{2q(d-d_1)})(1+e^{-2qd_1})}{e^{2q(d-d_1)}-e^{-2qd_1}}\right) = -\frac{1}{2}D^2 f(q)\Phi_q{}^2 \quad (15)$$

where $D^2 = \mu^2/2\epsilon_{\mathrm{membrane}}$ and $f(q) = q(((1 + e^{2q(d-d_1)})(1 + e^{-2qd_1}))/(e^{2q(d-d_1)} - e^{-2qd_1}))$. We can show numerically that, for length scales $\geq$100 nm, variation of the position of the flat plane changes $f(q)$ by less than 10%. Therefore, the position of the flat plane where the dipoles reside affects the long-range dipolar interactions in a minor way. For simplicity, we assume the dipole moments reside on the midplane $z = d/2$ and $f(q) = q((1 + e^{qd})(1 + e^{-qd}))/(e^{qd} - e^{-qd})$.

As $d \to \infty$, $F_{\mathrm{el}} \to -1/2\ D^2 q\Phi_q{}^2$, the electrostatic free energy is reduced to the completely unscreened long-range dipolar interactions in an infinitely large medium. This result was obtained by Andelman a long time ago.[30] As $d \to 0$, the term linear in q in the electrostatic free energy vanishes. Hence, the dipolar interaction between the helices becomes short-range in the limit of small membrane thickness, which corresponds to a physical system in which bare dipoles are surrounded by ionic solutions without any protection from the nonionic low-dielectric medium of the membrane. For finite membrane thickness d, although the presence of an ionic solution renormalizes the dipolar interactions between the helices within the membrane, as we will demonstrate below, the dipolar interactions remain long-range.

We also consider how the out-of-plane undulations of dipole positions affect the dipolar interaction. We assume that the position of the dipole moments is given by

$$z(x) = \frac{d}{2} + \Delta\sin\left(\frac{2\pi}{L}x\right) \quad (16)$$

We use perturbative methods to solve the same set of Poisson−Boltzmann equations (eqs 9−13) with the fluctuating boundary condition (eq 16). The free energy is

$$F = \int \mathrm{d}x \frac{1}{\sqrt{1+\frac{1}{2}\left(\frac{2\pi}{L}\Delta\right)^2}} P\left(E(x) + \Delta\sin\left(\frac{2\pi}{L}x\right)\frac{\partial E}{\partial x} + \frac{1}{2!}\Delta^2\sin^2\left(\frac{2\pi}{L}x\right)\frac{\partial^2 E}{\partial x^2} + \ldots\right) \quad (17)$$

$E(x)$ is the unperturbed electrical field, and $E(x) = \partial V_2/\partial z$ at $z = d/2$. For the case $L \gg 2\pi/q \approx 100$ nm, in which the undulation wavelength is much larger than the size of the domains in which dipoles reside. The above results for a flat plane will hold. For $L \ll 2\pi/q \approx 100$ nm, we can show that the free energy is asymptotically reduced by a factor of $(1 - (\pi\Delta/L)^2)$: $F_{\mathrm{el}}(q) \to (-1/2)D^2\Phi_q{}^2\ f(q)(1 - (\pi\Delta/L)^2)$. Intuitively, cell membranes appear like a sheet without width over the lateral length scale $>$ 100 nm; hence, the position variation within the membrane shall not affect the behavior very much over this or a larger lateral length scale. If $L = 10$ nm and $\Delta = 1$ nm, then the magnitude reduction of the dipolar interaction is less than 10%. Therefore, we ignore the out-of-plane undulation in the positions of dipole moments in our calculations.

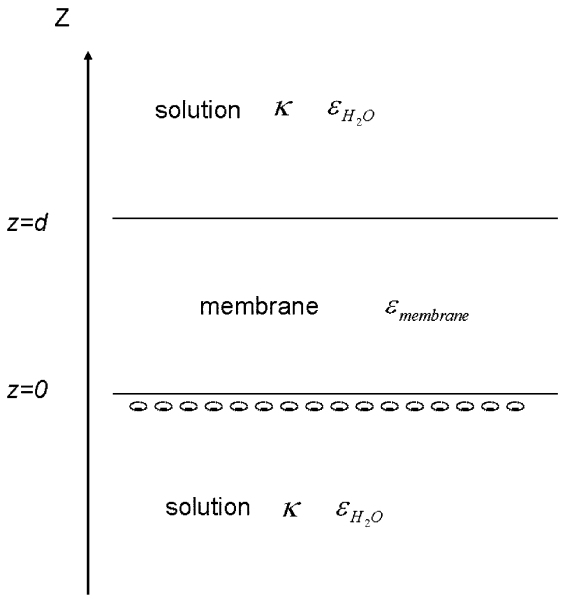

Figure 6. Schematic illustration of net surface charge on the membrane surrounded by the salty solution.

Appendix 2

Analysis of Net Negative Surface Charges on Cell Membranes. Consider the electrostatic interaction of a monolayer of charges residing on one side of the membrane, as shown in Figure 6. The electrical potentials are solved using the Poisson−Boltzmann equation

$$\nabla^2 V_1 - \kappa^2 V_1 = 0,\ z > d \quad (18)$$

$$\nabla^2 V_2 = 0,\ 0 < z < d \quad (19)$$

$$\nabla^2 V_3 - \kappa^2 V_3 = 0,\ z < 0 \quad (20)$$

with the boundary conditions

$$\text{(i)}\ \lim_{z\to\infty} V_1 = \lim_{z\to-\infty} V_3 = 0$$

$$\text{(ii)} V_1 = V_2,\ z = d$$

$$V_2 = V_3,\ z = 0$$

$$\text{(iii)}\ -\epsilon_{\mathrm{membrane}}\frac{\partial V_2}{\partial z} + \epsilon_{\mathrm{H_2O}}\frac{\partial V_3}{\partial z} = e\Phi_q e^{iqx},\ z = 0$$

$$-\epsilon_{\mathrm{membrane}}\frac{\partial V_2}{\partial z} + \epsilon_{\mathrm{H_2O}}\frac{\partial V_1}{\partial z} = 0,\ z = d$$

The electrostatic energy is

$$F_{\mathrm{el}}(q) = \frac{1}{2}e\Phi_q V(0) = \frac{1}{2}\frac{e^2\Phi_q{}^2}{\epsilon_{\mathrm{H_2O}}\sqrt{\kappa^2+q^2}}\left(\frac{(1-e^{-2qd}) + \frac{\epsilon_{\mathrm{membrane}}q}{\epsilon_{\mathrm{H_2O}}\kappa}(1+e^{-2qd})}{(1-e^{-2qd}) + 2\frac{\epsilon_{\mathrm{membrane}}q}{\epsilon_{\mathrm{H_2O}}\kappa}(1+e^{-2qd})}\right) \quad (21)$$

For the real system in which we are interested ($2\pi/q = 100-1000$ nm, $\kappa = 1\ \mathrm{nm}^{-1}$, $d = 5$ nm, $\epsilon_{\mathrm{membrane}} = 1-10$ and $\epsilon_{\mathrm{H_2O}} =$

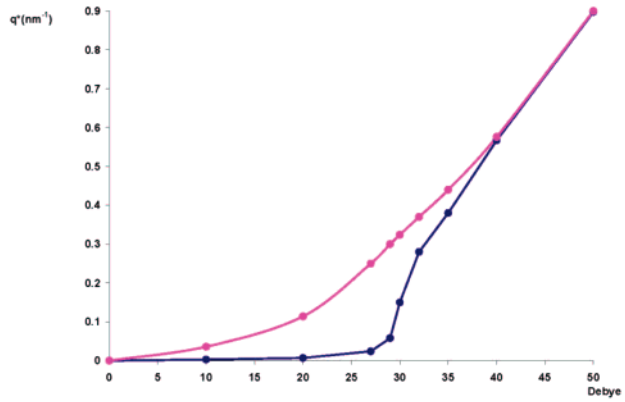

Figure 7. q^* vs dipole moment curves, the comparison between the screened dipole moment and the bare dipole moment. The line tension is $\gamma = 5k_BT$ for both cases. Pink curve: without the membrane confinement d. Blue curve: with the membrane confinement d ($d = 5$ nm).

$80, 1 \gg (1 - e^{-2qd}) \gg \epsilon_{membrane}q/\epsilon_{H_2O}\kappa$), the free energy reduces to

$$F_{el}(q) = \frac{1}{2}\frac{e^2\Phi_q^2}{\epsilon_{H_2O}\kappa}\left(1 - \frac{\epsilon_{membrane}q}{\epsilon_{H_2O}\kappa}\frac{(e^{qd} + e^{-qd})}{(e^{qd} - e^{-qd})}\right) = \frac{1}{2}(\text{const} - D^2 g(q))\Phi_q\Phi_{-q} \quad (22)$$

Where $D^2 = e^2\epsilon_{membrane}/\kappa^2\epsilon_{H_2O}$ and $g(q) = q(e^{qd} + e^{-qd})/(e^{qd} - e^{-qd})$. As the thickness of the membrane $d \to \infty$, we recover the results attributable to Andelman:[30] $F_{el} = (1/2)(\text{const} - D^2q)\Phi_q\Phi_{-q}$, which is equivalent to a dipolar interaction. For a finite membrane thickness, d, this dipolar interaction is modified by ionic screening effects.

Since the above two systems share a similar q-dependence on the (effective) dipolar interactions, we write their electrostatic free energies in the unified form

$$F_{el} = \frac{1}{2}\int d\vec{q}(\text{const} - D^2 f(q))\Phi_q\Phi_{-q} \quad (23)$$

To show that the (effective) dipolar interactions are still long-range interactions, we computed the optimal non-zero q^* that minimizes the quadratic term of the total free energy

$$F_{total} = \frac{1}{2}\int d\vec{q}(\gamma q^2 - D^2 f(q) + \text{const})\Phi_q\Phi_{-q}$$

Given the fixed line tension, the optimal q^* reflects the strength of the dipolar interactions (the larger the value of q^*, the stronger the dipole moment). To see how much the dipole moment is reduced because of screening effects, we numerically compare the above value of q^* with the one obtained from the free energy including the unscreened dipolar interaction

$$F_{total} = \frac{1}{2}\int d\vec{q}(\gamma q^2 - D^2 q + \text{const})\Phi_q\Phi_{-q}$$

According to Figure 7, for dipole moments above 30 D, the renormalized effective dipolar interaction is roughly the same as the unscreened dipolar interaction, as seen by $q^* = q_0^*$. On the other hand, smaller dipole moments are indeed reduced, since $q^* = q_0^*/10$.

Given typical values of line tensions, to form domains with a linear size ranging from micrometers to several tens of nanometers, the required dipole moment is on the order of several tens of debyes, which is within the physical range under physiological conditions. For the rest of the paper, to maintain simplicity of the model, we denote the long-range electrostatic interactions in the model system by the effective dipolar interactions

$$F_{el} = \frac{1}{2}\int d\vec{q}(\text{const} - D_{eff}^2 q)\Phi_q\Phi_{-q}$$

For brevity, in the main texts, we use D_i as D_{eff} for the effective dipole moment for species i.

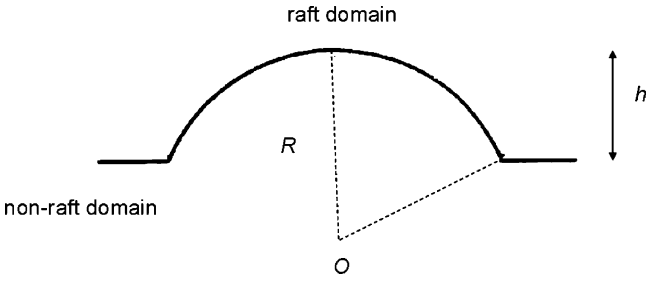

Figure 8. Schematic illustration of the raft domain geometry.

Appendix 3

Analysis of the Role of Spontaneous Curvature Differences between Raft and Nonraft Components. We assume that spontaneous curvature coupling with concentration fluctuations in the membrane is the only resource of long-range interactions. Consider the equilibrium shape of a raft domain surrounded by a nonraft domain under the influence of the bending energy and the line tension. The line tensions try to squeeze the domain so as to minimize the interface between the raft and nonraft domains. In other words, the line tension acts as a shrinking force to reduce the perimeter of the domain. At equilibrium, an expansion force normal to the perimeter of the domain is required to balance this shrinking force. This expansion force is provided only if the bending energy penalty tends to flatten the domain, which corresponds to the case in which the curvature of the domain is greater than the spontaneous curvature. Therefore, the curvature of the raft domain is the upper limit of the spontaneous curvature.

In the strong segregation limit, adopting Lipowski's theory,[43] the energy associated with the curvature of the domain is

$$E = \kappa\left(\frac{2}{R} - \frac{2}{R_0}\right)^2 2\pi Rh + 2\pi\gamma\sqrt{2Rh - h^2} + \Delta\sigma\pi h^2 + \Delta P\left(Rh^2 - \frac{1}{3}h^3\right)\pi \quad (24)$$

As shown in Figure 8, the curvature of the domain H is $2/R$, the spontaneous curvature of the raft component H_{sp} is $2/R_0$, and h is the height of the domain. The perimeter of the domain is $2\pi\sqrt{2Rh - h^2}$. The surface area is $2\pi Rh$. The volume of the bulge is $(Rh^2 - {}^1/_3h^3)\pi$. $\Delta\sigma$ is the surface tension difference between the raft and the nonraft domains. ΔP is the pressure difference between the outside and inside of the membrane. Under in vitro experimental conditions, the energy associated with the pressure difference is very small compared to other energy terms, so we ignore the last term in eq 24. When the energy is minimized with respect to the curvature ($2/R$), the equilibrium state requires $\partial E/\partial R = 0$, which yields $H = 2/R > H_{sp} = 2/R_0$. This result is essentially independent of the strong segregation limit, so we would expect that $H > H_{sp}$ still holds in the weak segregation limit.

In the weak segregation limit, the characteristic wavelength is given by

$$\frac{2\pi}{l^*} = \sqrt{\frac{\kappa H_{sp}\sqrt{\frac{\sigma}{\gamma}} - \sigma}{\kappa}}$$

Further, it yields

$$\frac{2\pi}{\sqrt{\frac{\kappa H\sqrt{\frac{\sigma}{\gamma}} - \sigma}{\kappa}}} < l^*$$

This is a necessary condition in that l^* is the minimal characteristic domain spacing that the model system must have if spontaneous curvature differences provide the main mechanism for lipid raft formation. Comparing our results with recent experiments on GUVs[23] in which $\sigma = 1.06 \times 10^{-7}$ to 8.6×10^{-8} N/m, $\kappa = 10^{-19}$ J, $\gamma = 9 \times 10^{-13}$ N, and $H = 0.96\ \mu m^{-1}$, the $2\pi/\sqrt{(\kappa H\sqrt{\sigma/\gamma} - \sigma)/\kappa}$ is $\sim$1.9 μm. This is much smaller than the observed domain size $l^* = 5.0\ \mu$m, which satisfies the necessary condition. Therefore, if the net surface charge density on the membrane is very low, spontaneous curvature coupling with concentration fluctuations could be the mechanism of lipid raft formation for synthetic membranes.

References and Notes

(1) Alberts, B.; Johnson, A.; Lewis, J.; Raff, M.; Roberts, K.; Walter, P. *Molecular Biology of the Cell*, 4th ed.; Garland Science: New York, 2002.

(2) Brown, D. A.; London, E. *Annu. Rev. Cell Dev. Biol.* **1998**, *14*, 111.

(3) Brown, D. A.; London, E. *J. Membr. Biol.* **1998**, *164*, 103.

(4) Simons, K.; Ikonen, E. *Nature* **1997**, *387*, 569.

(5) Simons, K.; Toomre, D. *Nat. Rev. Mol. Cell Biol.* **2000**, *1*, 31.

(6) Pierce, S. K. *Nat. Rev. Immunol.* **2002**, *2*, 96.

(7) Xavier, R.; Brennan, T.; Li, Q. Q.; McCormack, C.; Seed, B. *Immunity* **1998**, *8*, 723.

(8) Gaus, K.; Gratton, E.; Kable, E. P. W.; Jones, A. S.; Gelissen, I.; Kritharides, L.; Jessup, W. *Proc. Natl. Acad. Sci. U.S.A.* **2003**, *100*, 15554.

(9) Jordan, S.; Rodgers, W. *J. Immunol.* **2003**, *171*, 78.

(10) Harder, T.; Scheiffele, P.; Verkade, P.; Simons, K. *J. Cell Biol.* **1998**, *141*, 929.

(11) Janes, P. W.; Ley, S. C.; Magee, A. I. *J. Cell Biol.* **1999**, *147*, 447.

(12) Edidin, M. *Trends Cell Biol.* **2001**, *11*, 492.

(13) Verma, R.; Mayor, S. *Nature* **1998**, *394*, 798.

(14) Friedrichson, T.; Kurzchalia, T. V. *Nature* **1998**, *394*, 802.

(15) Dietrich, C.; Yang, B.; Fujiwara, T.; Kusumi, A.; Jacobson, K. *Biophys. J.* **2002**, *82*, 274.

(16) Pralle, A.; Keller, P.; Florin, E.-L.; Simons, K.; Horber, J. K. H. *J. Cell Biol.* **2000**, *148*, 997.

(17) Tokumasu, F.; Hwang, J.; Dvorak, J. *Langmuir* **2004**, *20*, 614.

(18) Tokumasu, F.; Jin, A. J.; Feigenson, G. W.; Dvorak, J. A. *Biophys. J.* **2003**, *84*, 2609.

(19) Johnson, K. G.; Bromley, S. K.; Dustin, M. L.; Thomas, M. L. *Proc. Natl. Acad. Sci. U.S.A.* **2000**, *97*, 10138.

(20) Call, M. E.; Pyrdol, J.; Wiedmann, M.; Wucherpfennig, K. W. *Cell* **2002**, *111*, 967.

(21) Estronca, L. M. B. B.; Moreno, M. J.; Abreu, M. S. C.; Melo, E.; Vaz, W. L. C. *Biochem. Biophys. Res. Commun.* **2002**, *296*, 596.

(22) Murase, K.; Fujiwara, T.; Umemura, Y.; Suzuki, K.; Lino, R.; Yamashita, H.; Saito, M.; Murakoshi, H.; Ritchie, K.; Kusumi, A. *Biophys. J.* **2004**, *86*, 4075.

(23) Baumgart, T.; Hess, S. T.; Webb, W. W. *Nature* **2003**, *425*, 821.

(24) Golestanian, R.; Goulian, M.; Kardar, M. *Phys. Rev. E* **1996**, *54*, 6725.

(25) Bruinsma, R.; Pincus, P. *Curr. Opin. Solid State Mater. Sci.* **1996**, *1*, 401.

(26) Ben-Tal, N.; Honig, B. *Biophys. J.* **1996**, *71*, 3046.

(27) Van Holde, K. E.; Johnson, W. C.; Ho, P. S. *Principles of Physical Biochemistry*; Prentice Hall: Upper Saddle River, NJ, 1998.

(28) Werlen, G.; Palmer, E. *Curr. Opin. Immunol.* **2002**, *14*, 299.

(29) Ottemann, K. M.; Xiao, W. Z.; Shin, Y. K.; Koshland, D. E. *Science* **1999**, *285*, 1751.

(30) Andelman, D.; Brochard, F.; Joanny, J. F. *J. Chem. Phys.* **1987**, *86*, 3673.

(31) Genet, S.; Costalat, R.; Jacques, B. *Biophys. J.* **2001**, *81*, 2442.

(32) Gilbert, D. L.; Ehrenstein, G. *Curr. Top. Membr. Transp.* **1984**, *22*, 407.

(33) Hille, B.; Woodhull, A. N.; Shapiro, B. I. *Philos. Trans. R. Soc. London, Ser. B* **1975**, *270*, 301.

(34) Rosenheck, K. *Biophys. J.* **1998**, *75*, 1237.

(35) Sheetz, M. P. http://www.columbia.edu/cu/biology/courses/g6002/2004/sheetz/lecture4.pdf (2004).

(36) Leibler, S.; Andelman, D. *J. Phys. II* **1987**, *48*, 2013.

(37) Safran, S. A. *Statistical Thermodynamics of Surfaces, Interfaces, and Membranes;* Westview Press: Boulder, CO, 1994.

(38) Simson, R.; Wallraff, E.; Faix, J.; Niewohner, J.; Gerisch, G.; Sackmann, E. *Biophys. J.* **1998**, *74*, 514.

(39) Bruinsma, R.; Behrisch, A.; Sackmann, E. *Phys. Rev. E* **2000**, *61*, 4253.

(40) Korlach, J.; Schwille, P.; Webb, W. W.; Feigenson, G. W. *Proc. Natl. Acad. Sci. U.S.A.* **1999**, *96*, 8461.

(41) Veath, S. L.; Keller, S. L. *Biophys. J.* **2003**, *85*, 3074.

(42) Brocca, P.; Cantu, L.; Corti, M.; Favero, E. D.; Motta, S. *Langmuir* **2004**, *20*, 2141.

(43) Lipowski, R. *J. Phys. II* **1992**, *2*, 1825.

(44) Dan, N.; Safran, S. A. *Biophys. J.* **1998**, *75*, 1410.

(45) Rietveld, A.; Simons, K. *Biochim. Biophys. Acta* **1998**, *1376*, 467.

(46) Dustin, M. L. *J. Clin. Invest.* **2002**, *109*, 155.

(47) Malinska, K.; Malinsky, J.; Opekarova, M.; Tanner, W. *Mol. Bio. Cell* **2003**, *14*, 4427.

(48) Bagnat, M.; Simons, K. *Proc. Natl. Acad. Sci. U.S.A.* **2002**, *99*, 14183.

(49) Radhakrishman, A.; Anderson, T. G.; McConnell, M. *Proc. Natl. Acad. Sci. U.S.A.* **2000**, *97*, 12422.

(50) Dykstra, M.; Cherukuri, A.; Sohn, H. W.; Tzeng, S.-J.; Pierce, S. K. *Annu. Rev. Immunol.* **2003**, *21*, 457.

(51) Zacharias, D. A.; Violin, J. D.; Newton, A. C.; Tsien, R. Y. *Science* **2002**, *296*, 913.